

Development of Background Flow Model of Hall Thruster Neutral Ingestion

IEPC-2017-008

*Presented at the 35th International Electric Propulsion Conference
Georgia Institute of Technology • Atlanta, Georgia • USA
October 8 – 12, 2017*

Jason D. Frieman¹, Thomas M. Liu², and Mitchell L.R. Walker³
Georgia Institute of Technology, Atlanta, Georgia, 30332, USA

The particle-based coupling between background gas flows in vacuum test facilities and neutral ingestion into Hall effect thrusters (HETs) is investigated. An analytical model of the facility background flow environment is developed to accommodate facilities with different geometries and pump placements as well as compute the ingested flow rate of background neutrals into a given HET. The ingested flow rates computed by the model are shown to predict previous empirical data taken using the 5-kW P5 and SPT-100 to within the experimental uncertainty. When compared to predictions generated assuming ingestion by the random flux of neutral particles, the ingested flow rates computed by the background flow model are shown to be 70% closer to the empirical measurements without requiring any semi-empirical inputs. It is also shown that the neutral ingestion at a fixed facility pressure can vary by as much as 91% suggesting that background pressure magnitude is an insufficient parameter for fully describing neutral ingestion effects. The results in this work indicate that the analytical background flow model is an effective predictive tool for computing neutral ingestion into HETs.

Nomenclature

A_{exit}	= thruster exit plane area, m ²
F_{S+}	= mass flow rate crossing surface S moving in the positive direction, kg/s
k	= Boltzmann's constant, J/K
m	= molecular mass of the background neutral, kg
\dot{m}	= net mass flow rate of gas, kg/s
\dot{m}_b	= net mass flow rate of bleed gas, kg/s
\dot{m}_{ing}	= ingestion mass flow rate of the background neutrals, kg/s
n	= number density, m ⁻³
n_b	= background neutral number density, m ⁻³
n_p	= number of active cryopumps
n_s	= number density of particles crossing surface S, m ⁻³

¹Graduate Research Assistant, Aerospace Engineering, High-Power Electric Propulsion Laboratory; currently Research Electrical Engineer, NASA Glenn Research Center; jfrieman3@gatech.edu.

²Research Engineer II, Aerospace Engineering, High-Power Electric Propulsion Laboratory; thomas.liu@ae.gatech.edu.

³Professor, Aerospace Engineering, High-Power Electric Propulsion Laboratory; mitchell.walker@ae.gatech.edu.

n_{S+}	= total number density of particles crossing surface S moving in the positive direction, m^{-3}
n_{S+i}	= number density of particles of population i crossing surface S moving in the positive direction, m^{-3}
n_{S-i}	= number density of particles of population i crossing surface S moving in the negative direction, m^{-3}
S	= surface area, m^2
S_c	= chamber cross-sectional area, m^2
S_{pd}	= total surface area of downstream pump surfaces, m^2
S_{pe}	= total surface area of end dome pump surfaces, m^2
S_{pu}	= total surface area of upstream pump surfaces, m^2
s_d	= ratio of total surface area of the downstream pump surfaces to the chamber cross-sectional area
s_e	= ratio of total surface area of the end dome pump surfaces to the chamber cross-sectional area
s_u	= ratio of total surface area of the upstream pump surfaces to the chamber cross-sectional area
T	= gas temperature, K
T_b	= temperature of the background neutrals, K
T_i	= temperature of particles of population i , K
T_p	= temperature of the pump surface, K
T_w	= temperature of the chamber wall, K
V_i	= thermal-diffusive velocity of particles of population i , m/s
V_s	= thermal-diffusive velocity of particles crossing surface S , m/s
α	= pump sticking coefficient
Φ	= ingestion flux due to random motion of background neutrals, $m^{-2}s$

I. Introduction

THE high specific impulse, thrust efficiency, and thrust density provided by Hall effect thrusters (HETs) make them an appealing choice for use as the primary propulsion system onboard increasing numbers of near-Earth satellite missions. In addition to the propellant mass savings offered by these performance attributes, developments in in-space power and the growing Western flight heritage portfolio of HETs have also increasingly made them prime candidates for more ambitious deep space missions.¹⁻³

The interest in these devices has caused a corresponding increase in the quantity of HET research and testing at numerous vacuum facilities. Despite the physical similarities among the HETs operated and characterized at each of these facilities, the wide range of facility geometries, sizes, materials, and pumping capacities makes it difficult for researchers to compare data sets without the inclusion of facility-dependent corrections.⁴ It is therefore necessary to develop an understanding of how to quantify ground-based vacuum facility effects on measured HET operation, thrust performance, and plume characterization so that facility-dependent testing artifacts can be corrected for and a facility-independent understanding of HET performance can be achieved.

Existing investigations focused on HET facility effects primarily focus on the impact of facility backpressure on plume properties and device performance. Previous studies have shown that increases in facility pressure result in artificial increases in device thrust and efficiency.⁵⁻²¹ This observed performance augmentation has been attributed to the ingestion of background neutrals present in the vacuum facility.⁵⁻²¹ In this process, background neutrals are entrained by the HET and used as propellant; thus, these neutrals are subsequently ionized and accelerated upon being ingested, but are not accounted for as part of the anode flow rate directly supplied to the HET.⁵⁻²¹ In many of these previous investigations, the entrainment of background neutrals is treated as the result of the random flux of these neutrals across the exit plane of the thruster (hereafter referred to as the thermal model).^{8,9,13,15,17,21} In the thermal model, the corresponding ingestion flux of background particles (Φ) can be expressed as a function of Boltzmann's constant (k) as well as the number density (n_b), temperature (T_b), and molecular mass (m) of the background neutrals using the following equation^{8,9,13-15,21}:

$$\Phi = \frac{1}{4} n_b \sqrt{8kT_b / \pi m} \quad (1)$$

The corresponding ingested mass flow rate of neutrals into the HET (\dot{m}_{ing}) can then be found as the multiplicative product of the ingestion flux from Eq. (1), the molecular mass of the background gas, and the thruster exit plane area (A_{exit}) as shown in Eq. (2)^{13,21}:

$$\dot{m}_{ing} = \Phi m A_{exit} \quad (2)$$

The thermal model has been successfully applied to explain trends observed in early empirical measurements of the SPT-100 HET and was used to generate the recommendation that all HETs be tested at a facility pressure below 5.0×10^{-5} Torr in order to keep background neutral ingestion below the threshold required to generate reliable predictions of in-orbit performance.^{13,17} However subsequent investigations with different HETs in different facilities have shown that the results generated by the thermal model under-predict the empirically-observed changes in discharge current (for cases of constant anode mass flow rate), required anode flow rate (for cases in which the discharge current was held constant), or thrust.^{8,9,14–16,21} Specifically, previous studies have shown that the ingestion mass flow rates predicted by the thermal model are 2-14 times too small to account for empirical observations.^{14,16,21} These under-predictions have prompted proposals replacing the exit plane area in Eq. (2) with a larger effective ingestion area to account for ionization of background neutrals in regions of the near-field plume where the electron temperature is still high enough to ionize the neutral gas.^{11,14,15} This approach has been disputed due to its reliance on the assumption that neutrals ingested across a reference surface in the plume are ionized equivalently to neutrals supplied through the HET gas distributor.^{6,15} Furthermore, although successfully applied to data taken with the 6-kW H6 in the Large Vacuum Test Facility (LVTF) at the University of Michigan, this approach has not yet been shown to be broadly applicable across multiple devices and facilities.^{6,15} Overall, these shortcomings prevent an accurate determination of HET flow ingestion and thus hinder the ability to accurately gauge changes in HET operating characteristics as a function of ingestion flow rate.^{8,9,14–16,21}

In addition to the aforementioned shortcomings, the thermal model assumes that all motion of background neutrals is random in nature. However, previous work modeling the rarefied background flow inside a HET test facility found that the background neutrals could not be treated simply as a static gas field with only thermal velocity components.^{22–24} Instead, it was found that an organized background flow field existed within the test facility during HET operation and that bulk axial velocities of over 100 m/s were achieved by the background neutrals.^{22,23} These models were successfully used to replicate the empirically-observed spatial pressure distribution within the LVTF as well as the VF-5 vacuum facility at NASA Glenn Research Center (GRC); however, only limited attempts have been made to apply these concepts to assess how the bulk flow of background neutrals could impact HET ingestion as well as explain previously acquired HET facility effects data.

This paper uses the bulk background flow modeling concepts first proposed by Cai *et al.* in order to predict the ingestion of background neutrals by a HET.²² The original model of the LVTF created by these researchers is further developed in order to accommodate facilities with different physical geometries and pump placements as well as directly compute the expected ingested mass flow rate of background neutrals by a given HET. The predictions of this expanded model are then compared to previous empirical data sets collected with two different thrusters in two different vacuum test facilities in order to evaluate the ability of the model to successfully predict empirical data. Finally, the background flow model is used to assess the impact of pressure modulation technique on neutral ingestion mass flow rate.

II. Background Flow Model

A. Overview of HET Vacuum Test Facilities

Fig. 1(a) shows a schematic of a typical vacuum test facility used for HET testing. These test facilities are usually stainless-steel cylindrical vacuum chambers measuring 4 m or more in length and 2 m or more in diameter equipped with cryopumps in order to achieve and maintain operating pressures on the order of 10^{-5} Torr or less.^{6,22,25–27} The cryopumps operate by cooling a plate or series of plates to an operating temperature of approximately 15 K using gaseous helium.²² When incident particles strike the pump surface, a fraction of the particles is condensed onto to the pump surface while the remaining particles reflect with a thermal speed characterized by the pump surface temperature.²² The probability that incident particles are condensed on the pump surface is known as the sticking coefficient (α), with the probability that an incident particle reflects off the pump expressed as $1-\alpha$.²² Thus, the sticking coefficient is a metric of pump performance and quantifies how effectively the pumps act as sinks of neutral particles from the background flow field.²² The number and location of these pumps vary between different facilities as does the facility geometry.^{6,22,28}

In operation, a HET is mounted inside the vacuum facility to a test stand typically located at one end of the facility. A low-density plasma flow (i.e., the HET plume) is then exhausted from the thruster in the axial direction towards the downstream end of the facility. Although some of the emitted ions and electrons recombine prior to striking the downstream facility surfaces, the ion-electron recombination mean free path is generally longer than the characteristic

axial facility dimensions; thus, most of these charged particles strike the downstream facility surfaces, recombine, and reflect as neutrals with a thermal speed characterized by the chamber wall temperature.^{22,25,28} Upon reflection, these neutrals are then able to traverse the vacuum facility until they strike and are condensed on one of the cryopumps. This motion of neutrals through the vacuum facility is known as the background neutral flow and is the focus of this model.

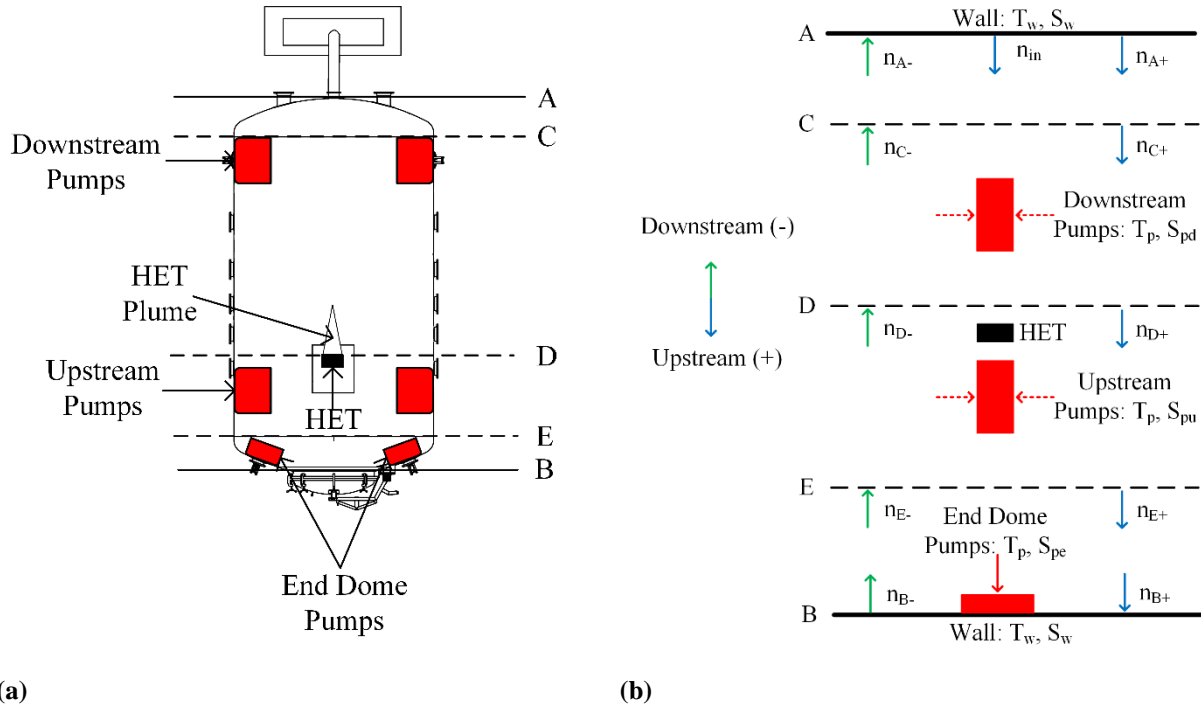


Fig. 1 (a) Schematic and (b) background flow model representation of a typical HET test facility.

B. Assumptions and Basic Relations

1. Assumptions

In order to model the flow environment described above, several simplifying assumptions were made. These assumptions, as well as the corresponding justifications underlying them, are detailed below.

The first set of assumptions concerns the background flow environment. First, it is assumed that the background flow in the test facility is in the free molecular regime. Previous work has shown that, because HET test facilities typically operate at pressures of 10^{-5} Torr-Xe or below, the Knudsen number in these facilities is of order unity.²² This is well within the range considered to be characteristic of a free molecular flow environment.²⁹ It is also assumed that the background flow is one-dimensional along the thrust axis of the HET. This assumption is consistent with previous studies into background neutral flows, which have yielded good agreement with more complex numerical simulations and empirical measurements.^{22,30,31} Finally, it is assumed that the background flow is in thermodynamic equilibrium. This implies all variables that impact the background flow (i.e., the temperatures of the chamber wall and pump surfaces as well as the anode mass flow rate) are in steady-state. This restricts the model to predictions of time-averaged ingestion flow rates. This restriction is appropriate for this model as the focus is on replicating empirical results acquired on the time scale of seconds to minutes (i.e., measurements of average discharge current and thrust) and not on the oscillation characteristics of HETs that occur at characteristic frequencies on the order of 20 kHz.³²

The next set of assumptions pertain to the vacuum test facility. Within the model, the chamber wall temperature and pump surface temperature are assumed to be constant and equal to 300 K and 15 K, respectively. For this work, the term “pump surface temperature” refers to the temperature of the helium cryosail and not the temperature of any liquid-nitrogen-cooled shrouds. The assumed pump surface temperature is consistent with reported empirical measurements in HET test facilities.²⁶ Furthermore, all cryopumps are assumed to have a constant sticking coefficient of between 0.25 and 0.4. It is important to note that typical values for the sticking coefficient of noble gases on bare cryogenic panels is typically within a range of 0.6 to 0.8.³³ However, since the pumps installed in many HET test facilities are surrounded by liquid-nitrogen-cooled, louvered shrouds, the effective sticking coefficient for these pumps

can be lower than the values achieved for a bare cryosurface; the assumed sticking coefficient range is in agreement with previous analytical and empirical studies of cryosurfaces with louvered shrouds.^{22,26} The sensitivity of the model to these assumptions are assessed in previous work.³¹

The final set of assumptions concerns the behavior of the individual particles composing the HET plume and background flow. First it is assumed that neutrals fully accommodate to the surfaces they strike and reflect specularly. Previous analysis has shown that the differences in results generated between diffuse and specular reflection assumptions are small; thus the impact of this assumption is expected to be minor.³⁰ Next, it is assumed that all particles injected into the HET anode travel unimpeded to the downstream facility surfaces, thermalize, and reflect. Thus, the downstream facility surfaces are considered as a source of neutral xenon entering the chamber at the thruster anode mass flow rate, through the chamber cross-sectional surface area, and at the wall temperature. This assumption is consistent with previous work into background flow modeling in HET test facilities.²² It is furthermore supported by empirical measurements of the velocity distributions within HET plumes; these measurements show that both ions and neutrals exhausted by the HET have large axial velocity components in the direction of the downstream chamber surfaces.³⁴ Further empirical evidence indicates that the majority of the ions are unlikely to undergo a recombination collision prior to reaching the downstream facility surfaces.²⁸ Thus, the most likely pathway for these particles to begin traveling back towards the thruster is by reflection from the downstream facility surfaces. It is nevertheless important to note that this assumption does not capture two processes present in facilities with downstream pumping surfaces. First, it does not capture the loss of unionized propellant exhausted by the HET due to contact with pump surfaces during the initial transit from the HET to the downstream facility surfaces. Second, it does not capture the effective reduction in chamber area caused by the shadowing of these downstream surfaces by the cryopumps. Fortunately, these processes have offsetting effects on the number density. Specifically, the first process reduces the effective number density of reflected neutrals while the second increases it.

Finally, it is assumed that the HET plume flow collisionally scatters background flow neutrals traveling towards the HET exit plane. The only collisions that are considered are the elastic collisions between the background neutrals and the unionized propellant exhausted by the HET. The collisional cross-sections are computed using models employed in previous HET plume models.³⁵ In order to compute the cross-sections, it was assumed that the neutral density at the exit plane of all HETs was approximately $1 \times 10^{18} \text{ m}^{-3}$; this estimate is taken from previous empirical measurements using the 1.5-kW SPT-100 and 5-kW P5 HETs, both of which are used as points of comparison for this work.^{35,36} The neutral density is furthermore assumed to follow an inverse-square dependency; this variation is derived by modeling the neutral density as the isotropic emissions of a rarefied flow from a disk with a diameter equal to the thruster exit area and is commonly applied in HET plume models.⁷ The velocity of plume neutrals is taken to be approximately 200 m/s, consistent with previous empirical measurements.³⁴ It is important to note that the large relative velocity (i.e., greater than 20,000 m/s) between the ions exhausted by the HET and the background neutral flows results in an elastic collisional cross-section more than an order of magnitude smaller than the computed cross-section for the elastic collisions between the background neutrals and the unionized propellant exhausted by the HET; thus this ion-neutral collision process is ignored for this work.

2. Basic Relations

Before the background flow model can be mathematically developed, a few basic relations regarding the flow of rarefied gas in equilibrium must be presented. The net mass flow rate (\dot{m}) of a rarefied gas across a surface in one direction for a one-dimensional flow is given by Eq. (3):

$$\dot{m} = mn_s S \sqrt{(8kT)/(\pi m)} / 4 = mn_{s+} S \sqrt{(2kT)/(\pi m)} \quad (3)$$

where S is the area of the surface, T is the temperature of the particles crossing the surface, and n_{s+} is the number density of particles crossing surface S moving in the positive direction (which is equal to half the total number density of particles at the surface as there are only two potential directions of motion), and all other variables retain their meaning from previous equations.²² The situation described by Eq. (3) is illustrated in Fig. 2.

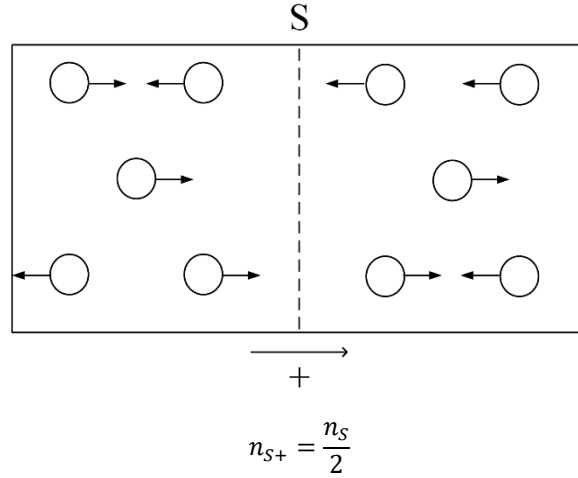


Fig. 2 One-dimensional motion of a rarefied gas.

For convenience, the simplified thermal-diffusive velocity term (V_s) from Eq. (3) will be defined as shown in Eq. (4):

$$V_s = \sqrt{(2kT)/(\pi m)} \quad (4)$$

Finally, from the law of mass conservation and Eq. (3), the number of particles of incoming temperature (T_1) reflected from a surface at a different temperature (T_2) is given by Eq. (5) ²²:

$$n_1 \sqrt{T_1} = n_2 \sqrt{T_2} \quad (5)$$

In Eq. (5) n_1 is the number density of the incoming particles, and n_2 is the number density of the reflected particles.

C. Model Development

Using the assumptions from Section II.B.1, the typical HET test facility shown in Fig. 1(a) is transformed into the 1-D background flow model shown in Fig. 1(b). In order to help correlate the model to the test facility, identical reference surfaces are drawn on both the schematic of the HET chamber shown in Fig.1(a) and the model representation in Fig. 1(b). These reference surfaces demarcate the different chamber regions of interest: the downstream wall region is located between surfaces A and C, the downstream pump region is located between surfaces C and D, the upstream pump region is located between surfaces D and E, and the end dome pump region is located between surfaces E and B. For this work, the dividing line between the upstream and downstream regions is the HET exit plane. In other words, all pumps located downstream of the HET exit plane and not on the end domes of the vacuum test facility are considered to be in the downstream pump region while those located upstream of the HET exit plane and not on the end domes of the vacuum test facility are considered to be in the upstream pump region. As shown in Fig. 1(b), because the model is one-dimensional, the number density of particles (and the corresponding flux) crossing each of these surfaces can be further decomposed into an upstream (i.e., positive) and downstream (i.e., negative) component.

The analytical model needed to compute the ingestion flow rate due to the background neutral flow is built from the identified assumptions, basic relations, and modeling domain. In order to arrive at this final solution, expressions for the flux and number density of background neutrals crossing each of the surfaces in both directions need to be obtained. These expressions can then be combined into a system of equations that can be solved for the ingestion number density (n_{D+}) and mass flow rate (F_{D+}). The model will be presented region-by-region in order to explicitly show the unique aspects associated with each type of region. Furthermore, the resulting equations will compose a toolkit that can readily be applied to build a model of any facility geometry or pump configuration.

1. Pump Regions

The model development starts by examining the flow environment in the upstream and downstream pump regions. There are three potential outcomes for background particles that enter a pump region: 1) the particles can proceed unimpeded through the region and exit at the temperature with which they entered, 2) the particles can strike a pump and condense, which removes them from the flow, or 3) the particles can strike a pump and reflect at the pump temperature. These outcomes are shown in Fig. 3.

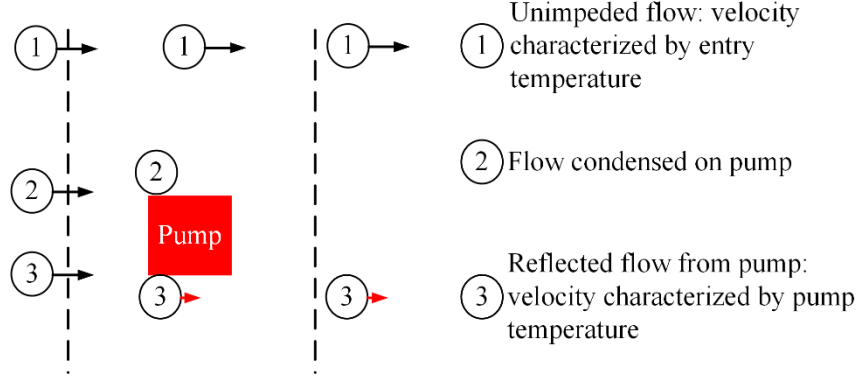


Fig. 3 Three potential outcomes for particles in pump regions.

Thus, the flow rate of particles of population i exiting the pump region (F_{D+i}) can be written as ²²:

$$F_{D+i} = mS_c n_{c+i} V_i - m S_{pd} n_{c+i} V_i + (1 - \alpha) n_{c+i} S_{pd} m V_p \sqrt{T_i/T_p} \quad (6)$$

Note that Eq. (6) is written using the flux across surface D in the positive direction as an example exit surface from a pump region. In Eq. (6), S_c is the chamber cross-sectional area, S_{pd} is the total surface area of cryopumps located in the relevant pump region (for this example it would be the downstream pump region), n_{c+i} is the number density of particles of population i entering the pump region (which, for this example, would be the number density of particles of population i crossing surface C in the positive direction), V_i is the thermal-diffusive speed characterized by the temperature of particles of population i (T_i), V_p is the thermal-diffusive speed characterized by the pump surface temperature (T_p), and all other terms retain their meanings from previous expressions.

Each of the summation terms in Eq. (6) represents one of the possible outcomes discussed above. The first term represents all particles that entered the pump region, the second term represents the particles that struck a pump surface, and the third term represents the fraction of particles that struck a pump surface but did not condense and instead reflected at a thermal-diffusive speed characterized by the pump surface temperature. Finally, it is important to note that Eq. (6) is also written for a single population of particles. If additional populations are entering the pump region, then Eq. (6) would be applied to each population and the total exit flow rate would be equal to the sum of the exit flow rates for each population. Such a situation could arise for adjacent pump regions (i.e., the upstream and downstream pump regions for a chamber similar to the one shown in Fig. 1(a)) as, after traversing the first pump region, the flux entering the second pump region would be composed of a population of particles at the original entry temperature and another at pump surface temperature made up of those particles that struck but were not trapped by a pump in the first pump region.

The number density of particles of population i exiting the pump region (n_{D+i}) can similarly be written as ²²:

$$n_{D+i} = (1 - s_d) n_{c+i} + (1 - \alpha) n_{c+i} s_d \sqrt{T_i/T_p} \quad (7)$$

In Eq. (7), s_d is the ratio of pump surface area to facility cross-sectional area in the region of interest, and all other terms retain their meaning from previous expressions. The first term of Eq. (7) represents the number density of particles that proceeded unimpeded through the pump region while the second is the number density of those that reflected from a pump and are now moving at a thermal-diffusive speed characterized by the pump surface temperature. As with Eq. (6), Eq. (7) is written for a single population of particles; the total exit number density would be equal to the sum of the number densities for each population.

2. Wall Regions

The next class of regions to consider are wall regions without end dome pumps. Such a region is shown between surfaces C and A in Fig. 1(b). All particles entering this region strike the facility walls, thermally accommodate to the facility wall, and then reflect with a thermal-diffusive speed characterized by the facility wall temperature. This process is shown in Fig. 4.

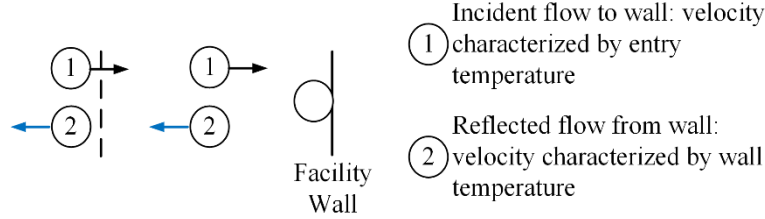


Fig. 4 Illustration of outcome for particles in wall regions.

The resulting exit flow rate can be expressed as ²²:

$$F_{C+i} = mS_c n_{A-i} V_w \sqrt{T_i/T_w} \quad (8)$$

The corresponding exit number density is ²²:

$$n_{C+i} = n_{C-i} \sqrt{T_i/T_w} \quad (9)$$

In Eq. (8) and Eq. (9), V_w is the thermal-diffusive speed characterized by the temperature of the chamber wall (T_w), and all other variables retain their meaning from previous expressions. As with Eq. (6) and Eq. (7), both Eq. (8) and Eq. (9) must be applied to all populations present, and the total mass flow rates and number densities will be the sum of the contributions of all populations and any source terms.

3. End Dome Pump Regions

The final type of facility region is an end dome pump region. Such a region is shown between surfaces E and B in Fig.1(b). Particles entering this region can either: 1) strike and thermally accommodate to the facility wall then reflect with a thermal-diffusive speed characterized by the facility wall temperature, 2) strike an end dome pump and condense, or 3) strike and thermally accommodate to an end dome pump then reflect with a thermal-diffusive velocity characterized by the pump surface temperature. These outcomes are illustrated in Fig. 5.

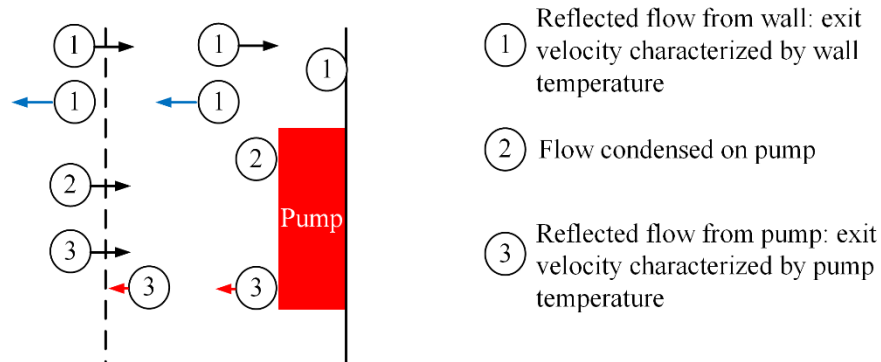


Fig. 5 Three potential outcomes for particles in end dome pump regions.

Thus, the number density of particles of population i exiting the end dome pump region (n_{E-i}) can be written as:

$$n_{E-i} = (1 - s_e) n_{E+i} \sqrt{T_i/T_w} + (1 - \alpha) n_{E+i} s_e \sqrt{T_i/T_p} \quad (10)$$

In Eq. (10), s_e is the ratio of pump surface area to facility cross-sectional area in the end dome pump region, and all other terms retain their meaning from previous expressions. The first term of Eq. (10) represents the number density of particles that strike the facility wall and are reflected with a thermal-diffusive speed characterized by the facility wall temperature, while the second term is the number density of reflected particles from a pump that are now moving at a thermal-diffusive speed characterized by the pump surface temperature.

4. Final Expressions

Application of Eq. (7), Eq. (9), and Eq. (10) to each of the reference surfaces shown in Fig. 1(b) results in a system of equations that can be solved simultaneously for the directional number densities crossing each surface. This system is shown for the positive directional number densities in Eq. (11)-(13). A similar system can be developed for the negative number densities crossing each surface.

$$n_{D+} = (1 - s_d)n_{C+} + (1 - \alpha)s_d n_{C+} \sqrt{T_w/T_p} \quad (11)$$

$$n_{E+} = n_{B+} = (1 - s_u)(1 - s_d)n_{C+} + (s_u(1 - s_d) + (1 - s_u)s_d + s_u(1 - \alpha)s_d)(1 - \alpha)n_{C+} \sqrt{T_w/T_p} \quad (12)$$

$$n_{C+} = n_{A+} = n_{in} - n_{C+}(\alpha s_d - 1)^2(\alpha s_e - 1)(\alpha s_u - 1)^2 \quad (13)$$

Since the HET exit plane is located just upstream of surface D, the parameter of interest for HET neutral ingestion is the mass flow rate of particles crossing surface D in the upstream direction (F_{D+}). The solution for this parameter is shown in Eq. (14)-(15):

$$n_{C+} = \frac{n_{in}}{1 + (\alpha s_d - 1)^2(\alpha s_e - 1)(\alpha s_u - 1)^2} \quad (14)$$

$$F_{D+} = m S_c n_{C+} V_w - m S_{p_d} n_{C+} V_w + (1 - \alpha)n_{C+} S_{p_d} m V_p \sqrt{T_w/T_p} \quad (15)$$

$$n_{in} = \frac{\dot{m}_{a,p}}{S_c} \quad (16)$$

In Eq. (11)-(15), s_u is the ratio of pump surface area-to-facility cross-sectional area in the upstream pump region, and all other terms retain their meaning from previous expressions. In Eq. (14), n_{in} is the input number density due to the HET anode flow computed as per the assumption regarding plume flow reflection in Section II.B.1. For clarity, this parameter is shown expressed as a function of the anode particle flow rate ($\dot{m}_{a,p}$) and the chamber cross-sectional area in Eq. (16). Since the HET exit plane occupies only a small fraction of the cross-sectional area of surface D, computing the actual ingested mass flow rate due to the background neutral flow requires the mass flow rate computed in Eq. (15) to be scaled by the ratio of the HET exit plane area to the cross-sectional area of the facility. This scaling ensures that only those particles that are on a trajectory to enter the HET channel are counted as part of the ingested mass flow rate.

Although developed for the chamber shown in Fig. 1(a), Eq. (14) can readily be modified to accommodate chambers of different geometric sizes and pump configurations by appropriately modifying the values of s_e , s_u , and s_d . For example, the result for a facility with no end dome pumps would be equal to Eq. (14) evaluated with s_e set to zero. Similarly, thrusters of different sizes or operating conditions can be accommodated by appropriately adjusting the exit area in the scaling mentioned above and the source term in Eq. (14).

As an initial test case, the above approach was applied in order to generate the form of Eq. (14) relevant to a facility with upstream pumps only. Such a facility matches the original model developed for the LVTF by Cai *et al.*²² By setting both s_e and s_d to zero (i.e., by removing the downstream and end dome pumps from the model), the empirically-validated expression developed by Cai *et al.* is indeed recovered.²² As an additional test case, the background flow model was used to compute the number density of particles crossing surface D in the positive direction assuming that both s_d and α were equal to one. This situation represents the limiting case of finding the number density remaining after a rarefied flow passes into a region occupied entirely by a pump surface onto which all incident particles condense. As expected, the model predicts that no particles would exit this region. These two test cases confirm both the accuracy of the math underlying the model and the above approach in expanding the background flow model to accommodate a wider variety of facility configurations.

Now that the final expressions of the model are developed, it is important to revisit the physical processes captured by Eq. (14)-(15) and how these processes might explain the empirically-observed enhancement in background neutral ingestion relative to the predictions of the thermal model. As described in detail in Section II.A, the physical process captured by this model is the reflection of the low-density plasma flow (as neutrals) from the downstream facility surfaces and their subsequent axial motion back towards the HET. This reflected motion is caused by the finite axial dimensions and pumping speed of the facility and represents a bulk motion towards the HET exit plane that could result in an additional or enhanced ingestion flux into the HET beyond that captured by the random motions of the thermal model. It is this additional flux (of the flow reflected off the downstream facility surfaces) that is captured by Eq. (15) and the concomitant enhancement of local number density that is captured by Eq. (14). Specifically, the velocity terms in Eq. (15) represent the bulk axial velocity of neutrals towards the HET exit plane due to reflection off of the facility surfaces.

It is furthermore important to note that this reflective process is not unique to HETs, but is widely applicable to any directional flow of a low-density plasma in a finite vessel, including the plume produced by gridded ion engines during ground testing. However, unlike in HETs (which have open channel exit areas in which ions are created), neutral ingestion into gridded ion engines is conductance-limited by the grid apertures.⁷ Thus, the bulk background flow is not able to freely stream into the ion engine discharge chamber and contribute to the plasma generation in this region. This significantly limits the impact of the bulk background flow on the ingestion characteristics of gridded ion engines and suggests the thermal model is sufficient for correcting the data acquired from these devices despite the model approximations.⁷

5. Comparisons to Existing Background Flow Models

Although the model developed in the preceding sections follows a similar approach to that taken by Cai *et al.*, it differs from this original model in several important ways.^{22,30,37} First, all models developed by Cai *et al.* have only a single pump region with a single type of pump (i.e., either end dome pumps exposed to the flow on only one side or upstream/downstream pumps exposed to the flow on two sides).^{22,30,37} Because of this, in those models, all particles enter the pump region with a uniform velocity characterized by the temperature of the facility walls.^{22,30,37} In contrast, the model developed in this work allows for the possibility of several adjoining pump regions of different types and thus the entrance of particles of several different populations with several different velocities into these regions. The ability to model adjoining pump regions and the corresponding discussion of how to account for these different populations is thus unique to this model and represents an increase in complexity over the original models developed by Cai *et al.*^{22,30,37} In addition, none of the original 1-D flow models created by Cai *et al.* account for the collisional scattering processes associated with the interaction of the background flow with the HET plume.^{22,30,37} These processes are accounted for in this work as described in Section II.B.1. It is important to note that many of the additional complexities accounted for in this model are also accounted for in the more complex direct simulation Monte Carlo (DSMC) models of the background flow environment in ground test facilities developed by Yim and Burt and Nakayama and Nakamura.^{23,24} However, in contrast to these DSMC models, the proposed 1-D model is much simpler to implement and customize to fit a given thruster and facility combination. To compare the two approaches (and therefore preliminarily assess the viability of the employed simpler approach), the background flow model was used to compute the weighted average speed of neutrals crossing surface D (i.e., those neutrals nearest the HET). These computations show a most-probable speed of approximately 100 m/s; this most-probable speed is in good agreement with the velocity distribution functions generated by the more complex DSMC codes.²³

The final difference between the model developed in this work and those previously developed lies in the application of the model results. The models developed by Cai *et al.*, Yim and Burt, and Nakayama and Nakamura were all used to create maps of the spatial neutral pressure distribution within ground test facilities.^{22-24,30,37} Although these results also indicated the presence of a bulk background flow of neutrals towards the thruster, to date, none of these models have been applied to compute the resultant ingestion mass flow rate into the HET due to this bulk motion nor have they been used to replicate existing empirical data sets quantifying the sensitivity of HETs to background pressure.

III. Comparisons to Empirical Data

In order to validate the applicability of the background flow modeling approach for predicting neutral particle ingestion by HETs, the model developed above was used to compute the ingested mass flow rates for situations identical to published experimental works on HET facility effects. These results were then compared against the empirical measurements of ingestion flow rate as well as the predictions of the thermal model.

When comparing the results of the background flow model to empirical measurements, it is assumed that background neutral particles ingested by the HET are ionized equivalently to neutrals supplied by the gas distributor. This simple ingestion approach is similar to that taken in many previous works on facility effects and is consistent with the approach taken in all of the works used for comparison.^{8,9,14-16,21} Furthermore, as mentioned above, only neutrals particles that cross the HET exit plane and enter the discharge channel are counted as part of the ingested mass flow rate in the background flow model. Since the mass flow in this region of the channel is free molecular, these neutral particles are free to travel into the ionization zone of the HET and are thus subject to collisions with the high-temperature electrons within this zone as are the neutrals supplied by the gas distributor.¹⁴

A. P5 HET in the LVTF

The first data used for model validation were collected using the P5 HET in the LVTF at the University of Michigan. The P5 is a laboratory-model Hall thruster developed jointly by the Air Force Research Laboratory (AFRL) and the University of Michigan.²¹ The P5 has a nominal operating power of 5 kW.²¹ The LVTF is a stainless-steel clad vacuum chamber measuring 9 m in length and 6 m in diameter and is equipped with seven cryopumps located upstream of the HET test station for a combined total upstream pump surface area of 7.26 m with a measured sticking coefficient of 0.4.^{2, 8,21,22}

The first data set used for validation was acquired by Hofer *et al.*⁸ In this work, the anode mass flow rate supplied to the P5 was varied in order to maintain a constant discharge current as the number of active pumps in the LVTF was varied from four to seven.⁸ The authors noted that higher anode mass flow rates were required to achieve a given discharge current at lower facility pressures and attributed the resultant change in required anode mass flow rate to a decrease in neutral ingestion.⁸ For instance, approximately 10 mg/s of anode flow was required, on average, to achieve a discharge current of 10 A in the four pump configuration, whereas 10.21 mg/s of anode flow was required, on average, in order to achieve the same discharge current in the seven pump configuration.⁸ Thus, the change in ingested mass flow rate between the two conditions can be approximated as 0.21 mg/s. The background flow model was similarly used to compute the difference in ingestion flow rate for the P5 in the LVTF as the number of active cryopumps was changed from four to seven. The results are shown as a function of anode flow rate along with the empirical results in Fig. 6(a). Also shown in Fig. 6(a) are the changes in ingestion flow rate predicted by the thermal model. Consistent with the approach taken in Hofer *et al.*, the number densities used for the thermal model calculations correspond to the average of the values acquired by a pair of hot-cathode ion gauges: one was located on the wall of the LVTF near the exit plane of the HET and the other was located on the wall at an axial distance equal to half the length of the LVTF.⁸ Previous work has shown that the pressures reported at these two locations in the LVTF vary by an average of 70%; the error bars shown for the thermal model predictions correspond to the uncertainty in the thermal model computations associated with this variance in the pressure measurements.³⁸ The error bars shown for the empirical data in Fig. 6 correspond to the reported uncertainty of the measurements.

As shown in Fig. 6(a), the changes in ingestion flow rate predicted by the thermal model are 7-15 times smaller than the empirical observations. However, the computed changes in ingestion flow rate generated by the background flow model are within the empirical error bars for all but one of the anode flow rates. For that flow rate (10 mg/s), there is less than a 10% difference between the upper uncertainty bound and the prediction of the background flow model. Thus, for this data set, the predictions generated by the background flow model are on average, 70% closer to the empirical values than the predictions generated by the thermal model.

It is important to note that the background flow model consistently over-predicts the change in ingestion mass flow rate for the 5 mg/s and 10 mg/s anode flow rates but under-predicts this change for the 12.5 mg/s and 15 mg/s anode flow rates. The reason for this is likely due to the employed collision model. As noted in Section II.B.1, neutral particles exhausted by the HET are assumed to travel at a constant speed regardless of the HET operating condition. However, HET wall and anode temperature have been empirically shown to increase with increasing discharge power.³⁹ This results in a corresponding increase in the temperature (and thus velocity) of unionized neutrals exhausted by the HET, with the corresponding reduction in the collisional cross-section for the modeled elastic collisions between the background neutrals and the unionized propellant exhausted by the HET.^{40,41} Since the background flow model does not capture this change in cross-section, it over-predicts the number of collisions that a background neutral undergoes (and thus under-predicts the ingestion flow rate) for operating conditions with high anode flow rates and vice versa for the low anode flowrate conditions.

In order to estimate the difference in operating characteristics between the LVTF and test conditions with no background pressure, Hofer *et al.* used the aforementioned data to generate linear fits that could be extrapolated to predict the anode flow rate that would be required to achieve a given discharge current in true vacuum conditions.⁸ The difference between this value and the anode flow rate required to achieve the same discharge current in the LVTF represents the ingested flow rate of neutrals by the P5 in the LVTF with all seven cryopumps operating. The

background flow model was similarly used to compute the ingestion flow rate for the P5 in the LVTF with all seven pumps on. The results are shown as a function of anode flow rate along with the empirical results in Fig. 6(b). As done by Hofer, *et al.*, the empirical data shown in Fig. 6(b) represents the average of the values acquired for each flow rate across four discharge voltages, while the error bars correspond to the standard deviation of these values.⁸ Also shown in the figure is the ingestion flow rate predicted by the thermal model for the P5 in the LVTF with all seven cryopumps operating. The number densities used for the thermal model calculations were determined identically the procedure described for the data shown in Fig. 6(a).⁸

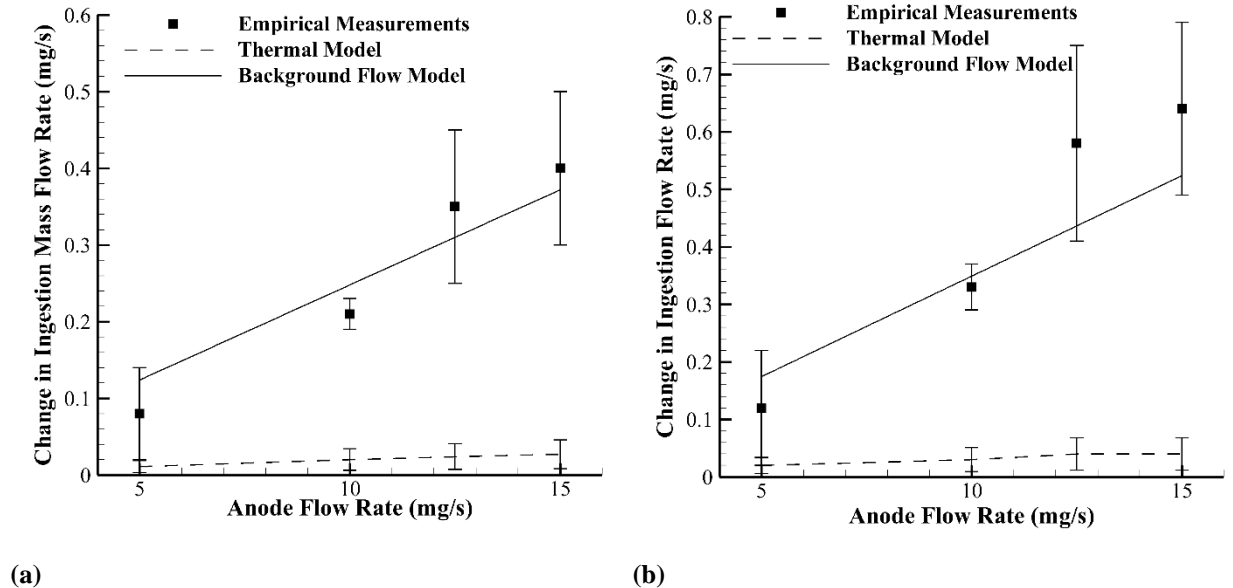


Fig. 6 Change in P5 ingestion flow rate between: (a) four and seven cryopumps and (b) seven cryopumps and vacuum.

As was the case for the data shown in Fig. 6(a), the results shown in Fig. 6(b) indicate that the predictions made by the background flow model are significantly closer to the empirical observations than the predictions generated using the thermal model. Specifically, the ingestion flow rates predicted by the thermal model are 11-24 times smaller than the empirical observations. By contrast, the difference between the estimates generated by the background flow model and the empirical measurements are less than the empirical error for all of the tested anode flow rates. Similar studies (omitted from this work for brevity) have shown the background flow model to offer similar increases in accuracy over the thermal model for additional empirical data acquired with the P5 in the LVTF by Walker and Gallimore as well as data acquired with the 6-kW H6 in the LVTF by Reid and the 1.35-kW SPT-100 HET by Diamant *et al.* in the vacuum facility at the Aerospace Corporation.^{6,14,15,21,31}

B. SPT-100

The background flow model matches empirical observations of enhanced ingestion. It is necessary to determine if it can replicate the original findings that Randolph *et al.* used to derive the thermal model.¹³ If these findings are successfully replicated, then the background flow model offers a framework to explain both the results observed by Randolph *et al.* and the enhanced ingestion rates observed in subsequent studies.^{8,9,14-16,21}

The SPT-100 testing performed by Sankovic *et al.* and analyzed by Randolph *et al.* was conducted in VF-5 at NASA GRC.^{13,42} VF-5 is 4.6 m in diameter and 19 m long and is equipped with a helium cryopump system surrounded by a liquid nitrogen-cooled shroud with an effective pumping area of 41 m², operating temperature of 20 K, and sticking coefficient of 0.25.^{13,42} Despite also being equipped with 20 diffusion pumps, only the cryopump system was employed during testing of the SPT-100. At the time of the SPT-100 performance evaluation, the entire cryopump system was located in the downstream section of the facility extending axially from the middle of the chamber to the downstream end dome.⁴²

In the data analyzed in the work of Randolph *et al.*, the sensitivity of the SPT-100 to facility background pressure was determined by measuring the change in average discharge current at a constant anode mass flow rate as the facility

pressure was varied using a bleed flow of propellant.^{13,42} The authors noted that higher average discharge currents were observed at higher facility pressures and attributed the resultant change in discharge current to an increase in neutral ingestion.^{13,42} The background flow model developed in Section II was similarly used to compute the change in ingestion mass flow rate relative to the baseline values obtained at the lowest operating pressure for the SPT-100 HET in the facility configuration used by Sankovic *et al.*⁴² The contributions to the change in ingestion mass flow rate from both the thermal and bulk motions of the facility background neutrals are shown as a function of facility pressure in Fig. 7.¹³ Consistent with the approach taken in Randolph *et al.*, the results are reported as the ratio of the ingestion mass flow rate to anode mass flow rate.¹³

Also shown in Fig. 7 are the empirical results from Sankovic *et al.*⁴² However, Sankovic *et al.* measured changes in mean discharge current as a function of facility pressure and thus did not directly obtain measurements of the ingestion mass flow rate.⁴ In order to compare these results to those generated using the background flow model, changes in discharge current must be related to the concomitant changes in ingestion mass flow rate. Using flow unit conversions, it can be shown that single ionization of 1 mg/s of xenon flow results in approximately 0.7 A of ion current.⁷ In HETs, the ratio of the ion beam current to the discharge current is typically on the order of 70% and has been shown to remain close to this value even at elevated ingestion mass flow rates; thus, an increase in ion current of approximately 0.7 A should result in a concomitant increase of 1 A in the discharge current.^{19,43} Thus, a 1 A increase in discharge current can be attributed to a 1 mg/s increase in ingestion mass flow rate. Previous work has indicated that the overall error associated with using this estimation technique to determine the change in ingestion mass flow rate is approximately 1%.³¹

As shown in Fig. 7, the ingestion flow rate into the SPT-100 HET due to the thermal motions of the background neutrals represents an average of 99% of the total ingestion flow rate across the full range of tested facility pressures. Thus, the background flow model predicts that, for the chamber configuration used to generate the data analyzed by Randolph *et al.*, the ingestion flow rate due to bulk motions of the background neutrals is negligibly small. This matches the key result presented by Randolph *et al.* that HET neutral ingestion could be modeled by considering only the thermal motions of the background neutrals. Taken together with the results from previous work in which the background flow model was able to successfully predict the enhanced neutral ingestion flow rates into a variety of other HETs and facilities, these results suggest that the physical mechanisms captured by the background flow model offer a framework to explain both the results observed by Randolph *et al.* and the enhanced ingestion rates observed in subsequent studies.^{8,9,14–16,21}

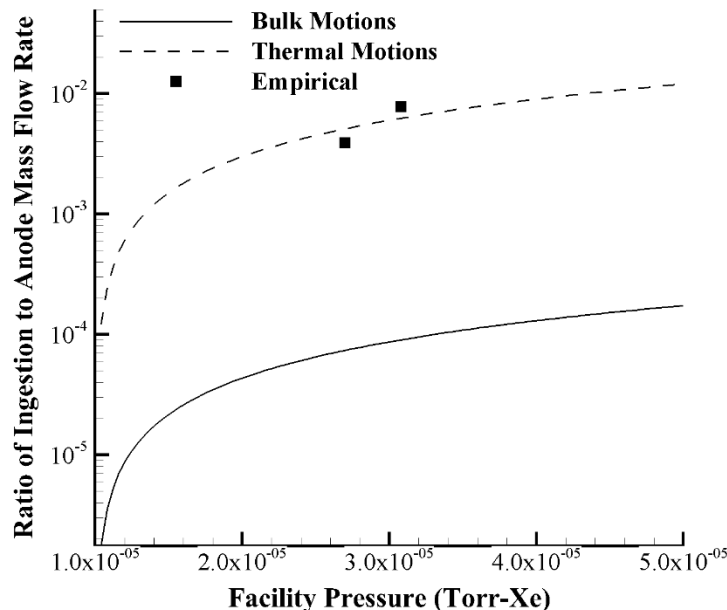


Fig. 7 Change in SPT-100 ingestion mass flow rate with facility pressure due to bulk and thermal motions of background neutrals

It is important to note that the orientation of the bleed flow inlet relative to the HET thrust vector is omitted from the published descriptions of the SPT-100 testing.^{13,42} Due to the one-dimensional nature of the background flow

model, radial injection of propellant cannot be directly modeled. Instead, the bleed flow was approximated as another source entering the chamber as per the assumption regarding plume flow reflection in Section II.B. Previous work has shown that this assumption causes an overestimation of the ingestion flow rate due to bulk motions of the background neutrals.³¹ This resultant overestimation due to the assumed axial orientation of the bleed flow inlet only further confirms the key result that, in the configuration analyzed by Randolph *et al.*, the background flow model correctly predicts that the contribution to the ingestion flow rate due to the bulk motions of the background neutrals is negligibly small.¹³

IV. Analysis of Pressure Modulation Techniques

As shown by the empirical data sets referenced in Section III, existing empirical investigations into HET facility effects change the nominal operating pressure in the test facility by some combination of varying the gas load via the introduction of a bleed flow of propellant and modulating the effective pumping speed by changing the number of active cryopumps.⁴⁴ However, since the nominal operating pressure in a HET test facility can be expressed as the ratio of the gas load to the effective facility pumping speed, there are many combinations of bleed flow rate and pumping speed that can yield a given operating pressure.⁴⁴ To illustrate this, the pressure in the LVTF during P5 operation at an anode flow rate of 10.46 mg/s was computed as a function of the number of active cryopumps and the bleed flow rate of propellant. The results are shown in Fig. 8. For these computations, it was assumed that the gas load of the P5 was 1.25 Torr-l/s and the nominal xenon pumping speed of the facility with all seven pumps on was 240,000 l/s. These numbers are consistent with values reported in previous investigations using the LVTF and were linearly scaled to account for the addition of bleed flow or the modulation of facility pumping speed²⁶. Using this approach, the pressure, P , that would be measured by an ion gauge mounted on the wall of the LVTF near the exit plane of the HET can be computed as a function of the bleed flow rate of propellant, \dot{m}_b , and the number of active pumps, n_p , using Eq. (17):

$$P = \frac{1.25 \left(\frac{\dot{m}_b + 10.46}{10.46} \right)}{240000 \left(\frac{n_p}{7} \right)} \quad (17)$$

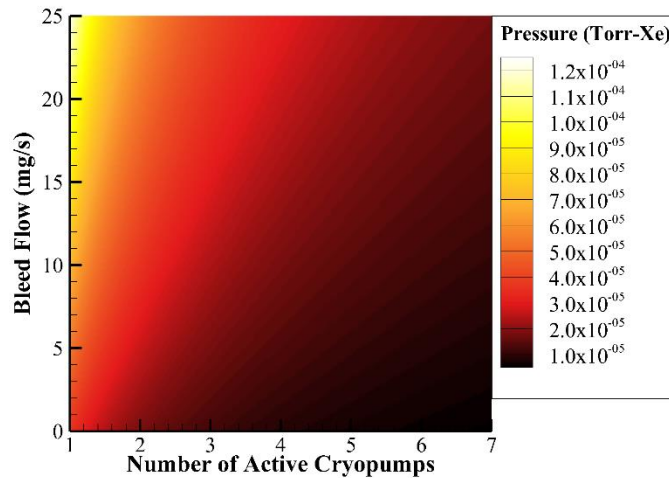


Fig. 8 LVTF operating pressure during P5 operation at an anode flow rate of 10.46 mg/s as a function of active pump quantity and bleed flow.

Despite the fact that each of the colored surfaces shown in Fig. 8 yield the same facility operating pressure, previous work has shown that the method used to achieve this pressure (i.e., the combination of bleed flow and pumping speed) can impact the concomitant response of the HET.^{9,23} In order to determine if HET neutral ingestion due to the bulk background flow is similarly affected by the method used to achieve a given facility pressure, the background flow model was used to compute the ingestion flow rate of neutrals into the P5 during operation at an anode flow rate of 10.46 mg/s in the LVTF for all combinations of bleed flow and pumping speed (i.e., number of active cryopumps) yielding a facility operating pressure of 2×10^{-5} Torr-Xe. The results are shown in Fig. 9. As done previously in the comparisons to empirical work with the SPT-100, the bleed flow was approximated as another source entering the chamber as per the assumption regarding plume flow reflection in Section II.B.1.

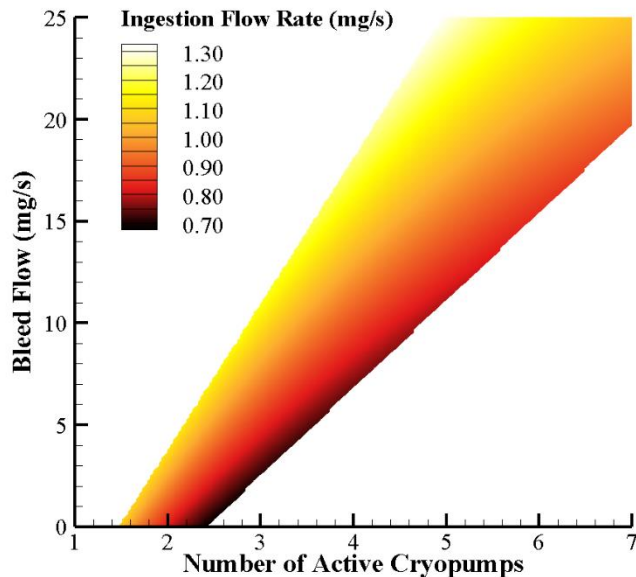


Fig. 9 Computed ingestion mass flow rates for P5 operation at an anode flow rate of 10.46 mg/s in the LVTF at a pressure of 2×10^{-5} Torr-Xe.

As shown in Fig. 9, at a fixed facility pressure of 2×10^{-5} Torr-Xe, the ingestion flow rate is not constant and varies depending on the combination of bleed flow and pumping speed used to achieve that pressure. Specifically, the ingestion flow rate varies from a minimum value of 0.69 mg/s (7% of the anode flow rate) to a maximum value of 1.31 mg/s (12.5% of the anode flow rate). The percent difference between these maximum and minimum possible ingestion flow rates is thus 91%. These changes in ingestion flow rate furthermore result in up to a 5.6% variation in total flow rate (i.e., the sum of the constant anode flow rate and ingestion flow rate) supplied to the HET. This variation is larger than the approximately 2% variation seen by Hofer *et al.* in Ref. 8 for the P5 in the LVTF when the facility pumping speed was halved and was achieved without changing the facility operating pressure. These results are furthermore consistent with previous works, which have shown that the background neutral distribution within the test facility and the HET ingestion characteristics vary depending on the method used to modulate the facility pressure.^{9,23} Overall, these results indicate that pressure magnitude is not a sufficient parameter in order to understand and predict neutral ingestion by a HET and that significant variation in total flow rate (or equivalently the discharge current) could be observed at a fixed facility pressure depending on how that pressure is achieved.

It is important to note that, in practice, many researchers orient bleed flows such that they are injected radially or in the cross-stream direction relative to the HET plume.^{6,14} However, as noted previously, because of the one-dimensional nature of the background flow model, this radial motion cannot directly be captured and all bleed flow is assumed to enter the facility traveling axially. This could cause the impact of bleed flow on ingestion flow rate to be overstated in the background flow model computations. To account for this, the ingestion flow rate was again computed assuming that only one-quarter of the bleed flow was traveling axially in the facility. This reduction in number density corresponds to assuming that the bleed flow motion is two-dimensional (i.e., can travel in the axial and radial directions) and that the bleed flow has an equal probability of traveling in any of these directions. Even with this reduction to account for the radial motion of the bleed flow, the results of the background flow model indicate up to a 4% variation in total flow rate supplied to the HET at a facility operating pressure of 2×10^{-5} Torr-Xe depending on how that pressure was achieved. This is still greater than the variation previously observed when the pumping speed in the LVTF was halved.⁸ Furthermore, this variation is observed at a pressure below the thresholds recommended Dankanich *et al.*²⁷

V. Conclusion

This work expanded the background flow modelling concept and explored the applicability of this approach to modeling neutral ingestion by HETs. The original modelling concept was further developed and generalized to

describe the background flow environment in facilities with any combination of end dome, upstream, and downstream pumps; in addition, analytic expressions were developed for the ingestion flow rate of a HET due to the background neutral flow within the facility. The predictions generated by these expressions were compared against empirical data taken with the P5 and SPT-100 HETs in two different facilities and found to match the empirical observations to within the experimental uncertainty. These predictions were furthermore shown to be 70% more accurate than those generated using the thermal model most commonly used to predict and estimate neutral ingestion by HETs without requiring any empirical inputs such as in-situ pressure measurements. The demonstrated improvement over the thermal model as well as the demonstrated accuracy in predicting empirical measurements for a variety of thrusters and facilities is, to the authors' knowledge, unique to the background flow model, thus lending credibility to this modeling approach and supporting its value as a predictive analytical tool. Furthermore, these results suggest that the physical mechanisms captured by the background flow model offer a framework to explain both the thermal ingestion results observed with the SPT-100 and the enhanced ingestion rates observed in subsequent facility effects studies.

The validated background flow model was used to assess the impact of pressure modulation techniques on HET neutral ingestion. It was shown that the ingestion flow rate of a HET can vary by as much as 91% at a fixed facility pressure of 2×10^{-5} Torr-Xe, depending on the combination of bleed flow and pumping speed used to achieve that pressure. Overall, these results indicate that pressure magnitude is not a sufficient variable for quantifying neutral ingestion by a HET, and that other test variables (i.e., pressure modulation technique) must be specified and held constant in order to fully describe HET ingestion characteristics.

References

¹Brophy, J.R., Friedman, L., and Culik, F., "Asteroid Retrieval Feasibility," *2012 IEEE Aerospace Conference*, IEEE, Piscataway, NJ, 2012, pp.1-16.

doi: 10.1109/AERO.2012.6187031

²Brophy, J. R., "Advanced Solar Electric Propulsion for Planetary Defense and Asteroid Resource Utilization," *34th International Electric Propulsion Conference*, Electric Rocket Propulsion Society, IEPC Paper 2015-065, Fairview Park, OH, 2015.

³Marchandise, F. R., and Koppel, C. R., "Electric Propulsion for deep space: a study case «Jupiter ICy Moon» with EP," *34th International Electric Propulsion Conference*, Electric Rocket Propulsion Society, IEPC Paper 2015-065, Fairview Park, OH, 2015.

⁴Semenkin, A., Kim, V., Gorshkov, O., and Jankovsky, R. "Development of Electric Propulsion Standards-Current Status and Further Activity," *27th International Electric Propulsion Conference*, Electric Rocket Propulsion Society, IEPC Paper 2001-070, Fairview Park, OH, 2001.

⁵Brown, D.L., and Gallimore, A.D., "Evaluation of Plume Divergence and Facility Effects on Far-Field Faraday Probe Current Density Profiles," *31st International Electric Propulsion Conference*, Electric Rocket Propulsion Society, IEPC Paper 2009-030, Fairview Park, OH, 2009.

⁶Diamant, K.D., Liang, R., and Corey, R.L., "The Effect of Background Pressure on SPT-100 Hall Thruster Performance," *50th AIAA/ASME/SAE/ASEE Joint Propulsion Conference & Exhibit*, AIAA Paper 2014-3710, 2014.

doi: 10.2514/6.2014-3710

⁷Goebel, D.M., and Katz, I., *Fundamentals of Electric Propulsion: Ion and Hall Thrusters*, Wiley, Hoboken, NJ, 2008, pp. 32-34, 325-384, 463-467.

⁸Hofer, R. R., Peterson, P. Y., and Gallimore, A. D., "Characterizing Vacuum Facility Backpressure Effects on the Performance of a Hall Thruster," *27th International Electric Propulsion Conference*, Electric Rocket Propulsion Society, IEPC Paper 2001-045, Fairview Park, OH, 2001.

⁹Hofer, R.R. and Anderson, J.R., "Finite Pressure Effects in Magnetically Shielded Hall Thrusters," *50th AIAA/ASME/SAE/ASEE Joint Propulsion Conference & Exhibit*, AIAA Paper 2014-3709, 2014.

doi: 10.2514/6.2014-3709

¹⁰Huang, W., Kamhawi, H., Lobbia, R.B., and Brown, D.L., "Effect of Background Pressure on the Plasma Oscillation Characteristics of the HiVHAc Hall Thruster," *50th AIAA/ASME/SAE/ASEE Joint Propulsion Conference & Exhibit*, AIAA Paper 2014-3708, 2014.

doi: 10.2514/6.2014-3708

¹¹Kamhawi, H., Huang, W., Haag, T., and Spektor, R., "Investigation of the Effects of Facility Background Pressure on the Performance and Voltage-Current Characteristics of the High Voltage Hall Accelerator," *50th AIAA/ASME/SAE/ASEE Joint Propulsion Conference & Exhibit*, AIAA Paper 2014-3707, 2014.

doi: 10.2514/6.2014-3707

¹²Nakles, M. R., and Hargus, W. A., "Background Pressure Effects on Ion Velocity Distribution Within a Medium-Power Hall Thruster," *Journal of Propulsion and Power*, Vol. 27, No. 4, 2011, pp. 737-743.

doi:10.2514/1.48027

¹³Randolph, T., Kim, V., Kaufman, H. R., Kozubsky, K., Zhurin, V. V., and Day, M., "Facility Effects on Stationary Plasma Thruster Testing," *23rd International Electric Propulsion Conference*, Electric Rocket Propulsion Society, IEPC Paper 1993-093,

Fairview Park, OH, 1993.

¹⁴Reid, B. M., "The Influence of Neutral Flow Rate in the Operation of Hall Thrusters," Ph.D. Dissertation, Aerospace Engineering Dept., Univ. of Michigan, Ann Arbor, MI, 2009, pp. 306–319.

¹⁵Reid, B. M., "Empirically-Derived Corrections for Facility Effects in Performance and Plume Measurements of Hall Thrusters," *34th International Electric Propulsion Conference*, Electric Rocket Propulsion Society, IEPC Paper 2015-362, Fairview Park, OH, 2015.

¹⁶Tighe, W. G., Spektor, R., Diamant, K., and Kamhawi, H., "Effects of Background Pressure on the NASA 173M Hall Current Thruster Performance," *34th International Electric Propulsion Conference*, Electric Rocket Propulsion Society, IEPC Paper 2015-152, Fairview Park, OH, 2015.

¹⁷Byers, D., and Dankanich, J., "A Review of Facility Effects on Hall Effect Thrusters," *31st International Electric Propulsion Conference*, Electric Rocket Propulsion Society, IEPC Paper 2009-076, Fairview Park, OH, 2009.

¹⁸Crofton, M. W., and Pollard, J., "Thrust Augmentation by Charge Exchange," *49th AIAA/ASME/SAE/ASEE Joint Propulsion Conference & Exhibit*, AIAA Paper 2013-4131, 2013.

doi: 10.2514/6.2013-4131

¹⁹Diamant, K., Spektor, R., Beiting, E., Young, J., Curtiss, T., and Corporation, T. A., "The Effects of Background Pressure on Hall Thruster Operation," *48th AIAA/ASME/SAE/ASEE Joint Propulsion Conference & Exhibit*, AIAA Paper 2012-3735.

doi: 10.2514/6.2012-3735

²⁰Huang, W., Kamhawi, H., and Haag, T., "Effect of Background Pressure on the Performance and Plume of the HiVHAc Hall Thruster," *33rd International Electric Propulsion Conference*, Electric Rocket Propulsion Society, IEPC Paper 2013-058, Fairview Park, OH, 2013.

²¹Walker, M.L.R., and Gallimore, A.D., "Performance Characteristics of a Cluster of 5-kW Laboratory Hall Thrusters," *Journal of Propulsion and Power*, Vol. 23, No. 1, 2007, pp. 35–43.

doi: 10.2514/1.19752

²²Cai, C., Boyd, I. D., and Sun, Q., "Free molecular background flow in a vacuum chamber equipped with two-sided pumps," *Journal of Vacuum Science & Technology A: Vacuum, Surfaces, and Films*, Vol. 24, No. 1, 2006, pp. 9-19.

doi: 10.1116/1.2126678

²³Yim, J. and Burt, J.M., "Characterization of Vacuum Facility Background Gas Through Simulation and Considerations for Electric Propulsion Ground Testing," *51st AIAA/SAE/ASEE Joint Propulsion Conference*, AIAA Paper 2015-3825, 2015.

doi: 10.2514/6.2015-3825

²⁴Nakayama, Y. and Nakamura, M., "Electric Propulsion Propellant Flow within Vacuum Chamber," *34th International Electric Propulsion Conference*, Electric Rocket Propulsion Society, IEPC Paper 2015-360, Fairview Park, OH, 2015.

²⁵Frieman, J. D., King, S. T., Walker, M. L., and Khayms, V., "Preliminary Assessment of the Role of a Conducting Vacuum Chamber in the Hall Effect Thruster Electrical Circuit," *50th AIAA/ASME/SAE/ASEE Joint Propulsion Conference & Exhibit*, AIAA Paper 2014-3712, 2014.

doi: 10.2514/6.2014-3712

²⁶Walker, M. L. R., "Effects of Facility Backpressure on the Performance and Plume of a Hall Thruster," Ph.D. Dissertation, Aerospace Engineering Dept., Univ. of Michigan, Ann Arbor, MI, 2005, pp. 111-155.

²⁷Dankanich, J., Walker, M. L. R., Swiatek, M., and Yim, J., "Recommended Practice for Pressure Measurements and Calculation of Effective Pumping Speeds during Electric Propulsion Testing," *33rd International Electric Propulsion Conference*, Electric Rocket Propulsion Society, IEPC Paper 2013-358, Fairview Park, OH, 2013.

²⁸Frieman, J. D., King, S. T., Walker, M. L. R., Khayms, V., and King, D., "Role of a Conducting Vacuum Chamber in the Hall Effect Thruster Electrical Circuit," *Journal of Propulsion and Power*, Vol. 30, No. 6, 2014, pp. 1471–1479.

doi: 10.2514/1.B35308

²⁹Anderson, J. D., *Fundamentals of Aerodynamics*, McGraw-Hill Education, New York, NY, 2010, pp. 54-57.

³⁰Cai, C., "Theoretical and Numerical Studies of Plume Flows in Vacuum Chambers," Ph.D. Dissertation, Aerospace Engineering Dept., Univ. of Michigan, Ann Arbor, MI, 2005 pp. 22-76.

³¹Frieman, J. D., Liu, T. M., and Walker, M.L.R., "Background Flow Model of Hall Thruster Neutral Ingestion," *Journal of Propulsion and Power*, 2017.

doi: 10.2514/1.B36269

³²Choueiri, E. Y., "Plasma oscillations in Hall thrusters," *Physics of Plasmas*, Vol. 8, No. 4, 2001, pp. 1411–1426.

doi: 10.1063/1.1354644

³³Ketsdever, A. D., "Design Considerations for Cryogenic Pumping Arrays in Spacecraft–Thruster Interaction Facilities," *Journal of Spacecraft and Rockets*, Vol. 38, No. 3, 2001, pp. 400–410.

doi: 10.2514/2.3698

³⁴Cedolin, R. J., Hargus, W. A., Storm, P. V., Hanson, R. K., and Cappelli, M. A., "Laser-induced fluorescence study of a xenon Hall thruster," *Applied Physics B: Lasers and Optics*, Vol. 65, No. 4, 1997, pp. 459–469.

doi: 10.1007/s003400050297

³⁵Boyd, I.D., "A Review of Hall Thruster Plume Modeling," *38th Aerospace Sciences Meeting and Exhibit*, AIAA Paper 2000-0466, 2000.

doi: 10.2514/6.2000-466

- ³⁶Walker, M.L.R., and Gallimore, A.D., “Neutral density map of Hall thruster plume expansion in a vacuum chamber,” *Review of Scientific Instruments*, Vol. 76, No. 5, 2005, Paper 053509.
- ³⁷Cai, C., Boyd, I., and Sun, Q., “Rarefied Background Flow in a Vacuum Chamber Equipped with One-Sided Pumps,” *Journal of Thermophysics and Heat Transfer*, Vol. 20, No. 3, Jul. 2006, pp. 524–535.
doi: 10.2514/1.19178
- ³⁸Walker, M., Gallimore, A., Cai, C., and Boyd, I., “Pressure Map of a Facility as a Function of Flow Rate to Study Facility Effects,” *38th AIAA/ASME/SAE/ASEE Joint Propulsion Conference and Exhibit*, AIAA Paper 2002-3815, 2002.
doi: 10.2514/6.2002-3815
- ³⁹Martinez, R., Dao, H., Walker, M., and Tech, G., “Power Deposition into the Discharge Channel of a Hall Effect Thruster,” *Journal of Propulsion and Power*, Vol. 30, No. 1, Jan. 2014, pp. 209–220.
doi: 10.2514/1.B34897
- ⁴⁰Boyd, I. D., and Dressler, R. A., “Far Field Modeling of the Plasma Plume of a Hall thruster,” *Journal of Applied Physics*, Vol. 92, No. 4, 2002, pp. 1764–1774.
doi: 10.1063/1.1492014
- ⁴¹Reid, B. M., and Gallimore, A. D., “Review of Hall Thruster Neutral Flow Dynamics,” *30th International Electric Propulsion Conference*, Electric Rocket Propulsion Society, IEPC Paper 2007-038, Fairview Park, OH, 2007.
- ⁴²Hofer, R., “Development and Characterization of High-Efficiency, High-Specific Impulse Xenon Hall Thrusters,” Ph.D. Dissertation, Aerospace Engineering Dept., Univ. of Michigan, Ann Arbor, MI, 2004, pp. 67-69.
- ⁴³Sekerak, M. J., “Plasma Oscillations and Operation Modes in Hall Effect Thrusters,” Ph.D. Dissertation, Aerospace Engineering Dept., Univ. of Michigan, Ann Arbor, MI, 2014, pp. 55-58.
- ⁴⁴Dushman, S., and Lafferty, J. M., *Scientific Foundations of Vacuum Technique*, Wiley, New York, 1962, pp. 347-374.